

# Heavy metal sensors and sequestering agents based on polyaromatic copolymers and hydrogels

Aula A Alwattar,<sup>a,b\*</sup> Athir Haddad,<sup>a,b</sup> Joshua Moore,<sup>a</sup> Mubark Alshareef,<sup>a,c</sup> Cian Bartlam,<sup>d</sup> Adam W Woodward,<sup>a,e</sup> Louise S Natrajan,<sup>a,e</sup> Stephen G Yeates<sup>a</sup> and Peter Quayle<sup>a</sup>



## Abstract

A series of readily available, amphiphilic pyrene- and perylene-containing fluorescent materials, derived from the copolymerisation of 2-acrylamido-2-methyl-1-propanesulfonic acid with acrylate esters, can be used to detect heavy metal ions in the micromolar concentration range in aqueous solutions. The incorporation of these amphiphilic copolymers into semi-interpenetrating hydrogels also resulted in the irreversible removal of divalent  $\text{Co}^{2+}$ ,  $\text{Ni}^{2+}$ ,  $\text{Cu}^{2+}$  and  $\text{Pb}^{2+}$  ions from aqueous solutions at neutral pH.

Supporting information may be found in the online version of this article.

**Keywords:** polyaromatic copolymers; amphiphilic polymers; free radical polymerisation; IPNs; detector and hazardous metals

## INTRODUCTION

Tackling pollution and waste management continues to be of major concern to environmental scientists, the manufacturing sector, regulatory bodies and the general public.<sup>1</sup> The presence of heavy metals in the environment, which exude from a variety of sources ranging from the weathering of rocks, to mining and wastewater discharge, poses a particular threat to the biosphere given the toxicity of these species to biota in the millimolar concentration range.<sup>2,3</sup> Industrial wastewater streams may contain a variety of heavy metals such as  $\text{Cu}^{2+}$ ,  $\text{Co}^{2+}$ ,  $\text{Pb}^{2+}$ ,  $\text{Ni}^{2+}$  and  $\text{Hg}^{2+}$  whose detection and removal is required prior to discharge into the environment.

Although many methods, such as atomic absorption spectroscopy, X-ray absorption spectroscopy and inductive coupled plasma atomic emission spectrometry, have been developed for trace metal analysis,<sup>4–7</sup> their high cost, complex sample preparation and the time consuming nature of their application limits their general use.<sup>8</sup> Consequently, a fluorescence-based detection technique has attracted considerable attention among the optical sensors.<sup>9</sup>

In a similar vein the fluorescence response of both low molecular weight organic molecules and polymers to the presence of heavy metals has been extensively investigated as an analytical tool for trace metal analysis.<sup>10</sup> This methodology is compromised, however, by issues of low sensitivity and poor water solubility of many organic fluorophores which limits their use for the detection of metal ions in aqueous media.<sup>11–15</sup> It is noted that highly

fluorescent pyrene and perylene derivatives have been used widely as sensors due to their high sensitivity to heavy metals even at low concentrations.<sup>16</sup> For example, perylene-3,4,9,10-tetracarboxylic dianhydride and its derivatives, which possess high fluorescence efficiency and excellent thermal and light stabilities,<sup>17,18</sup> have been successfully utilised as fluorometric and colourimetric sensors for  $\text{Cu}^{2+}$ ,  $\text{Ni}^{2+}$  and  $\text{Fe}^{3+}$  in dimethylformamide (DMF).<sup>19–21</sup>

Associated with the need for the development of analytical protocols for heavy and transition metal ion detection is the identification of reliable methods for their remediation from aqueous solutions. In the past this has been achieved by the use of adsorbents which incorporate polar functionality such as sulfonic

\* Correspondence to: AA Alwattar, Department of Chemistry, the University of Manchester, Manchester, M13 9PL, UK. E-mail: aula.alwattar@manchester.ac.uk

a Department of Chemistry, University of Manchester, Manchester, UK

b Chemistry Department, College of Science, University of Basrah, Basrah, Garmat Ali, Iraq

c Department of Chemistry, Faculty of Applied Science, Umm Al-Qura University, Makkah, Saudi Arabia

d Department of Materials and the National Graphene Institute, University of Manchester, Manchester, UK

e Photon Science Institute, University of Manchester, Manchester, UK

acids,<sup>22</sup> carboxylic acids<sup>22,23</sup> and amines<sup>23</sup> which are able to ligate metal ions. These systems enable metal ion removal via chelation and ion exchange mechanisms which prove to be superior compared to a simple sorption process. In the case of sorbents, the selectivity of metal ion uptake and of sorption capacity of the sorbent material may be difficult to rationalise<sup>24</sup> due to the subtle interplay between functional groups attached to the sorbent and coordination properties of individual metal ions.<sup>25,26</sup>

Hydrogels<sup>22,27</sup> having porous crosslinked polymeric structures and high surface areas are also known to adsorb heavy metal ions and radionuclides.<sup>28–33</sup> It has been shown, for example, that poly(acrylic acid-co-acrylamide) hydrogels are able to selectively sequester  $\text{Cu}^{2+}$  in the presence of other metal ions from aqueous streams.<sup>34</sup> Numerous studies have also shown that the incorporation of 2-acrylamido-2-methyl-1-propanesulfonic acid (AMPS) into a hydrogel facilitates metal ion binding, as illustrated by the use of a poly(2-acrylamido-2-methyl-1-propanesulfonic acid-co-vinyl imidazole) hydrogel for the removal of  $\text{Cu}^{2+}$  and  $\text{Fe}^{2+}$  from aqueous waste streams.<sup>35</sup> Similarly, a series of chitosan and acrylamide hydrogels were prepared as heavy metal adsorbents. These hydrogels have low adsorption capacity (typically  $3.29 \text{ mg g}^{-1}$  with efficiencies  $e$  of  $>90\%$ ), where the affinity for divalent metal ions was found to follow the trend  $\text{Pb}^{2+} > \text{Cu}^{2+} > \text{Co}^{2+} > \text{Ni}^{2+}$  which became optimum at basic pH.<sup>36</sup> Spherical hydrogel particles were prepared from chitosan and gelatin and showed effective non-selective removal of heavy metal ions ( $\text{Pb}^{2+}$ ,  $\text{Hg}^{2+}$ ,  $\text{Cd}^{2+}$  and  $\text{Cr}^{3+}$ ) from a simulated industrial waste stream.<sup>37</sup> In a similar vein, and in a drive towards a greener economy, the synthesis of soybean-derived hydrogels, capable of removing  $\text{Cd}^{2+}$  and  $\text{Pb}^{2+}$  (to a maximum adsorption of  $1.43$  and  $2.04 \text{ mmol g}^{-1}$ ) from aqueous solutions, has recently been reported.<sup>38</sup> Despite these advances, the identification of readily available, low-cost and high efficiency metal-selective adsorbents which operate at near-neutral pH remains an important goal.<sup>39</sup>

In the present study we report an operationally simple method for the synthesis of water soluble, fluorescent, pyrene and perylene copolymers derived from the free radical copolymerisation of AMPS in the presence of either 5-(perylene-3-yl)pent-4-yn-1-yl methacrylate or 1-pyrenemethyl methacrylate.<sup>40–43</sup> To the best of our knowledge, the synthesis and subsequent utilisation of these copolymers for the spectrophotometric detection of heavy metals has not been previously reported. In addition these copolymers were formulated into interpenetrating polymer network (IPN) hydrogels to investigate the effect of the presence of potentially self-associating polyaromatic groups on the swelling effect and ultimate metal uptake of the ionisable AMPS residue ( $\text{p}K_{\text{a}}$  ca  $1.5$ )<sup>35</sup> from aqueous solutions at ambient temperatures and neutral pH.<sup>39</sup> The physical properties of these hydrogels were fully characterised using TGA, DSC and rheometry, while surface morphologies were investigated by SEM.

## EXPERIMENTAL

### General methods

Matrix-assisted laser desorption/ionization (MALDI) mass spectra were acquired recorded on a Shimadzu Axima Confidence instrument using a dithranol matrix. High-resolution mass spectra were obtained using a Thermo Exactive Plus EMR or Thermo Finnigan MAT95XP mass spectrometer.

$^1\text{H}$  NMR (500 MHz) spectra were recorded using a Bruker Avance II<sup>+</sup> spectrometer referencing to the residual protons in  $\text{CDCl}_3$  (7.27 ppm) or deuterated dimethyl sulfoxide ( $\text{DMSO-d}_6$ ) (2.50 ppm).  $^{13}\text{C}$  NMR

spectra (126 MHz) were recorded using a Bruker Avance II<sup>+</sup> spectrometer referencing to the residual solvent peak as appropriate:  $\text{CDCl}_3$  (77.00 ppm),  $\text{DMSO-d}_6$  (39.51 ppm). Coupling constants ( $J$ ) are reported in hertz and chemical shifts ( $\delta$ ) are reported in parts per million. Signal multiplicities are designated as singlet (s), doublet (d), triplet (t), quartet (q), multiplet (m) or any collection of these.

IR spectra were recorded using a Thermo Scientific Nicolet iS5 spectrometer with an iDS ATR accessory in the solid state.

UV-visible spectra were recorded using a Varian Eclipse 5000 spectrophotometer between 200 nm and 800 nm using quartz cuvettes with a path length of 1 cm. Fluorescence spectra were recorded with a Varian Eclipse fluorescence spectrometer and performed under aerated conditions. Samples were irradiated ( $\lambda_{\text{ex}} = 340$  and  $420$  nm) in quartz cuvettes (1 cm) and the emission wavelength was recorded between 300 and 600 nm. Steady state emission spectra were recorded on an Edinburgh Instruments FP920 Phosphorescence Lifetime Spectrometer equipped with a 450 W steady state xenon lamp (with single 300 mm focal length excitation and emission monochromators in Czerny–Turner configuration) and interchangeable EPL pulsed diode laser excitation sources and a red sensitive photomultiplier in a Peltier (air cooled) housing (Hamamatsu R928P) detector. Lifetime data were recorded following excitation with an EPL laser using time correlated single photon counting. Lifetimes were obtained by a reconvolution fit using the instrumental response, and quality of fit was judged by minimization of reduced  $\chi$ -squared and residuals squared.

Gel permeation chromatography (GPC) was used to determine the molecular weight of the copolymers in  $0.1 \text{ mol L}^{-1}$  disodium hydrogen phosphate and azide with a flow rate of  $0.5 \text{ mL min}^{-1}$  ( $1\text{--}2 \text{ mg mL}^{-1}$ ) at  $40^\circ\text{C}$  using a refractive index detector. The system was calibrated with polyethylene oxide, in the range 200 to  $6 \times 10^6 \text{ g mol}^{-1}$ . DSC measurements were obtained with a TA DSC-250 under a nitrogen atmosphere ( $50 \text{ mL min}^{-1}$ ) at a heating rate of  $10^\circ\text{C min}^{-1}$  from 0 to  $145^\circ\text{C}$ .

Field emission SEM was carried out on Au/Pd coated cryogenically fractured hydrogel samples. Samples were freeze dried prior to examination. All samples were examined in high vacuum with 5 kV accelerating voltage on a Zeiss Ultra microscope with an in-lens detector. Image analysis was carried out using BoneJ software (University of Manchester).<sup>44</sup>

Rheological characterisation was carried out using an ARES LN2 rheometer (TA Instruments, Hertfordshire, UK) with parallel-plate geometry of 25 mm diameter. Test methods of oscillatory strain sweep and frequency sweep were used. Strain sweep tests were performed at a constant temperature ( $20.0^\circ\text{C}$ ) using a frequency of 1.0 Hz and a strain increase from 1% to 100% (or the maximum range permitted where this was lower) with recording of the corresponding stress, storage modulus ( $G'$ ) and storage and loss modulus ( $G''$ ). From these data the linear viscoelastic region was identified.

Frequency sweeps were performed at a constant strain within the linear viscoelastic region. The oscillatory frequency was then increased from 0.1 to 5.0 Hz in a steady ramp whilst recording the complex viscosity ( $\eta^*$ ),  $G'$  and  $G''$  data as a function of frequency. A  $\tan \delta$  value was calculated from these data.

### Materials

All reactants, reagents and dry solvents were purchased from Merk (Gillingham, UK), Acros Organics and Fisher Scientific (Loughborough, UK) and were used without further purification except for 2,2'-azobis(2-methylpropionitrile) (AIBN) which was

recrystallised from methanol prior to use. Thin-layer chromatography (TLC) was carried out using DC-Fertigfolie POLYGRAM® SIL G/UV254 precoated TLC sheets with substrate detection by UV light (254 and 365 nm).

## Synthesis

### Synthesis of perylene-5-ylpent-3-yne-2-methylprop-2-enoate (PePnUMA) (monomer)

To a solution of 5-(perylene-3-yl)pent-4-yn-1-ol<sup>45</sup> (740 mg, 2.2 mmol) and Et<sub>3</sub>N (0.9 mL, 6.6 mmol) in dry CH<sub>2</sub>Cl<sub>2</sub> (20 mL) was added, dropwise, via a syringe, methacryloyl chloride (0.6 mL, 6.6 mmol) under an atmosphere of dry nitrogen and the reaction mixture was then allowed to warm to room temperature with stirring for 24 h. The insoluble salts that were generated were then removed by filtration at the pump, and the solid residue was washed with ether (30 mL). The combined organic extracts were washed (HCl (2 mol L<sup>-1</sup>, 2 × 50 mL), 5% aqueous NaHCO<sub>3</sub> (75 mL) and then brine (75 mL)), dried (MgSO<sub>4</sub>) and concentrated *in vacuo*. Recrystallization of the residue from methanol afforded 5-(perylene-3-yl)pent-4-yn-1-yl methacrylate (PePnUMA) (485 mg, 1.2 mmol, 55% yield), as a fluorescent golden/brown-coloured solid, melting point 150–153 °C.

<sup>1</sup>H NMR (500 MHz, CDCl<sub>3</sub>) δ ppm: 1.57 (br, s, 1 H, O–H), 1.99 (s, 3 H, C=C–CH<sub>3</sub>), 2.13 (quin, *J* = 6.6 Hz, 2 H, C–C–H), 2.74 (t, *J* = 7.1 Hz, 2 H, C=C–C–H), 4.41 (t, *J* = 6.3 Hz, 2 H, O–C–H), 5.59 (s, 1 H, C=C–H), 6.17 (s, 1 H, C=C–H), 7.48 (td, *J* = 7.8, 2.8 Hz, 2 H, Ar–H), 7.56 (t, *J* = 7.9 Hz, 1 H, Ar–H), 7.61 (d, *J* = 7.8 Hz, 1 H, Ar–H), 7.69 (d, *J* = 8.1 Hz, 2 H, Ar–H), 8.10 (d, *J* = 7.8 Hz, 1 H, Ar–H), 8.14–8.25 (m, 4 H, Ar–H). <sup>13</sup>C NMR (126 MHz, CDCl<sub>3</sub>) δ: 16.8, 18.4, 28.1, 63.5, 79.7, 94.74, 119.6, 120.5, 120.6, 120.7, 120.8, 125.6, 126.1, 126.5, 126.6, 127.1, 127.9, 128.1, 128.4, 128.5, 130.8, 131.1, 131.2 and 131.4 (due to accidental equivalence only 16 aromatic carbons are reported rather than 20 expected for this structure) (see Fig. S1). Mass spectrometry (MS): *m/z* (MALDI, dithranol) 402.4 ([M]<sup>+</sup> 100%), 425.3 ([M + Na]<sup>+</sup> 85%). IR  $\bar{\nu}_{\text{max}}$ /cm<sup>-1</sup>: 3050 (Ar C–H), 2963 and 2902 (C–H), 2350 (C≡C), 1701 (C=O), 1289 (Ar C=C), 1167 (C–O–C). High resolution MS (HESI<sup>+</sup>): [C<sub>29</sub>H<sub>22</sub>O<sub>2</sub>K]<sup>+</sup> requires 441.1251, found 441.1235. The emission spectra for PyMA and PePnUMA are shown in Fig. S2.

### Polymer synthesis

Synthesis of poly(pyren-1-ylmethyl-2-methylprop-2-enoate-co-2-methyl-2-(prop-2-enoylamino) propane-1-sulfonic acid (PyMA-co-AMPS) (CoP1). PyMA-co-AMPS was prepared by a slight modification of a literature procedure.<sup>40,46</sup>

A solution of 1-pyrenemethyl methacrylate<sup>47</sup> (176 mg, 0.6 mmol) and 2-acrylamido-2-methyl-1-propanesulfonic acid (607 mg, 2.9 mmol) in dry DMF (10 mL) was degassed (three freeze–thaw cycles) and heated to 60 °C under dry nitrogen. Purified AIBN (7.8 mg, 1% compared to monomer weight) was then added to this solution and the reaction mixture was heated to 75 °C for 24 h. On cooling to ambient temperature (23 °C) the reaction mixture was poured into cold (0 °C) ethyl acetate (750 mL) and the precipitated polymer was collected at the pump and washed successively with diethylether (100 mL), CH<sub>2</sub>Cl<sub>2</sub> (100 mL) and finally acetone (100 mL). Precipitation (twice from MeOH into ethyl acetate) was used to further purify the copolymer which was recovered by filtration and dried under vacuum affording a beige solid (705 mg, 80% yield). The <sup>1</sup>H NMR and <sup>13</sup>C NMR spectra of this copolymer are shown in Figs 1(A), S3 and S5 (in Appendix S1). Repeating this copolymerization reaction procedure using different monomer feed ratios while maintaining a constant

AIBN amount (1% mol of the total two monomer weight) afforded copolymers CoP1-1, CoP1-2 and CoP1-3, as detailed in Table 2.

Synthesis of poly(peryene-5-ylpent-3-yne-2-methylprop-2-enoate-co-2-methyl-2-(prop-2-enoylamino) propane-1-sulfonic acids (PePnUMA-co-AMPS) (CoP2). This copolymer was prepared, using the procedure outlined above, starting from 5-(perylene-3-yl)pent-4-yn-1-yl methacrylate (118 mg, 0.3 mmol) and AMPS (60 mg, 2.9 mmol) and afforded the copolymer CoP2 as a brown greenish-coloured solid (85.8 mg, 43% yield). Repeating this copolymerization reaction procedure using different monomer feed ratios while maintaining constant AIBN amount (1% mol of the total two monomer weight) afforded copolymers CoP2-1, CoP2-2 and CoP2-3, as detailed in Table 2.

### Preparation of IPN hydrogels

A general method for the preparation of hydrogels is as follows: CoP2-3 (0.2 g), acrylamide (5 g), hydroxyethylmethacrylate (HEMA) (2 g) and methylene bis-acrylamide (0.72 g, 10% compared to monomer) were dissolved in 15 mL deionised (DI) water. To this homogeneous solution was then added ammonium persulphate (200 µL of a 10% w/v aqueous solution) and *N,N,N',N'*-tetramethylethylenediamine (TMEDA) (25 µL) and the reaction mixture was stirred at room temperature for 10 min in order for the polymerisation reaction to go to completion. This general process was repeated for a series of polymerization reactions as detailed in Table 1. In all of these examples methylene bis-acrylamide was used as a crosslinking agent (10% w/w with respect to monomer) and TMEDA (25 µL) was used as accelerant. AH21 and AH22 were prepared as controls. The resulting hydrogels were dried and washed three times with water to remove any monomer residue, filtered and dried under vacuum at 30 °C.

The swelling ratio for all these hydrogels was determined by immersing 1 g of the hydrogel in 50 mL of metal ion solution (Pb<sup>2+</sup>, Cu<sup>2+</sup>, Ni<sup>2+</sup> and Hg<sup>2+</sup>, 18 mg L<sup>-1</sup>) for 72 h. The swelling ratio (SR) was determined using the equation

$$\text{SR (\%)} = \frac{W_s - W_d}{W_d} \times 100 \quad (1)$$

where  $W_s$  is the mass of swollen hydrogels and  $W_d$  is the mass of dried hydrogels.<sup>48,49</sup>

### Metal ion uptake and release study

The dried hydrogel (0.3 g) was immersed in metal ion solutions: Pb<sup>2+</sup>, Cu<sup>2+</sup>, Ni<sup>2+</sup> and Co<sup>2+</sup> (15 mL, 18 mg L<sup>-1</sup>) for 72 h, without agitation or stirring, at room temperature. The concentration of metal ions which was not absorbed by the hydrogel was determined using inductively coupled plasma spectroscopy (ICP).

The metal uptake was calculated using the equation

$$\text{metal ion uptake (\%)} = \frac{C_0 - C_e}{C_0} \times 100 \quad (2)$$

where  $C_0$  and  $C_e$  are the initial and equilibrium concentration (in mg L<sup>-1</sup>) of metal ion remaining in solution.<sup>49,50</sup>

Each hydrogel–metal complex was then re-immersed in DI water (25 mL) for 72 h, without agitation or stirring, at room temperature. A sample of the aqueous solution was then analysed using ICP in order to measure the leached metal ion concentrations.

The desorption ratio<sup>45</sup> for each sample could be calculated as follows:

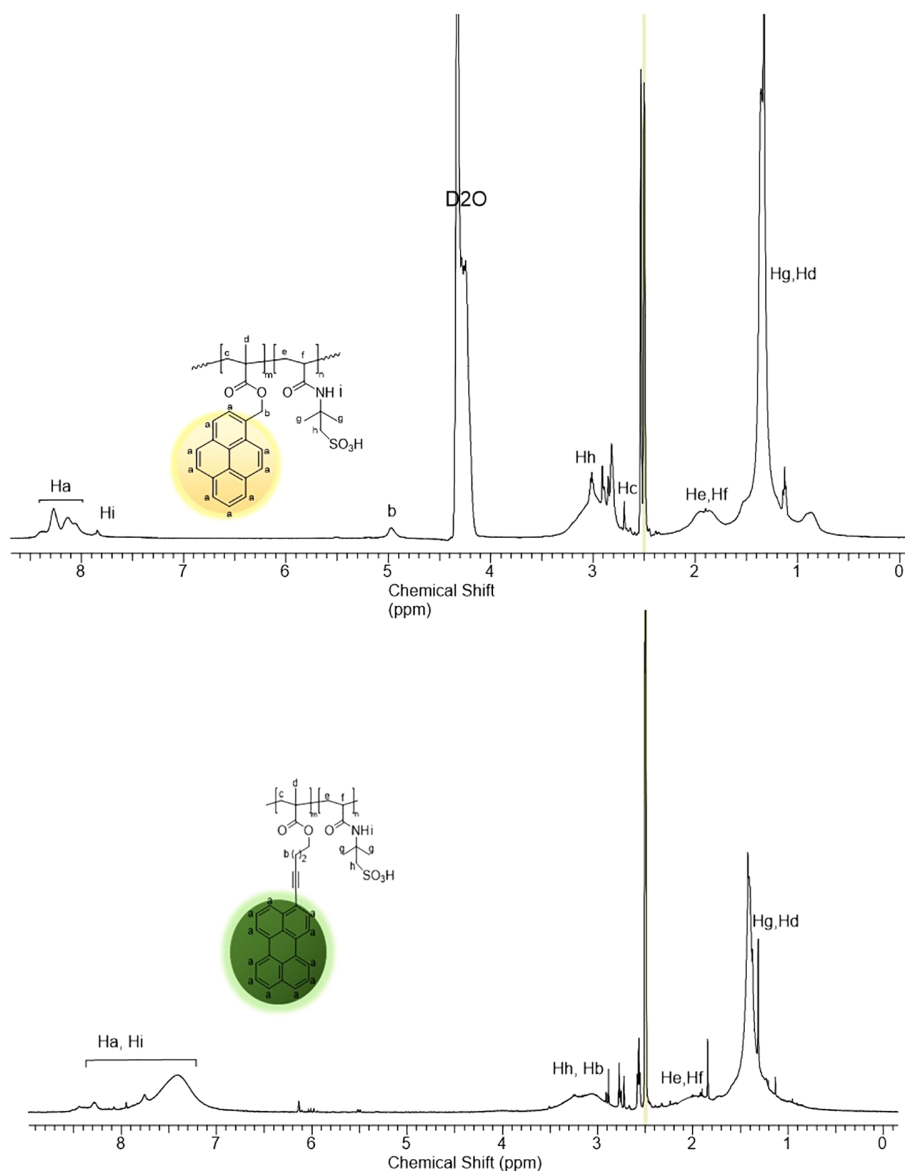


**Figure 1.**  $^1\text{H}$  NMR (500 MHz,  $\text{DMSO-d}_6$ ) of (A) CoP1-1 (top) and (B) CoP2-1 (bottom).

$$\text{desorption ratio} = \frac{W_d}{W_b} \times 100 \quad (3)$$

where  $W_d$  and  $W_b$  are the amount of metal ion desorbed into solution and the amount of metal ion bound to hydrogels (in  $\text{mg L}^{-1}$ ) respectively.

In passing we note that *in situ* hydrogel formation was also briefly investigated using aqueous solutions of  $\text{Pb}^{2+}$  ( $7.1 \mu\text{mol L}^{-1}$ ). This process led to the direct encapsulation of the metal ion into the hydrogel matrix where the metal ion appeared to be resistant to leaching once placed in fresh DI water.

#### UV-visible and fluorescence studies

Fluorometric titrations were also conducted on CoP2-3 after exposure to aqueous solutions of various metal ions. In these experiments solutions of  $\text{Co}^{2+}$ ,  $\text{Ni}^{2+}$  (as  $\text{CoCl}_2$  and  $\text{NiCl}_2$ ),  $\text{Hg}^{2+}$  (as  $\text{Hg}(\text{O}_2\text{CCH}_3)_2$ ),  $\text{Pb}^{2+}$  (as  $\text{Pb}(\text{NO}_3)_2$ ),  $\text{Na}^+$ ,  $\text{Mg}^{2+}$  and  $\text{Cu}^{2+}$  (as  $\text{Na}_2\text{SO}_4$ ,  $\text{MgSO}_4$  and  $\text{CuSO}_4$ ) ( $0.1\text{--}5 \text{ mL}$ ,  $0.01 \text{ mmol L}^{-1}$  in DI water) were added to CoP2-3 ( $2.0 \text{ mL}$ ,  $0.01 \text{ mmol L}^{-1}$  in DI water) in a quartz

cuvette. These reaction mixtures were shaken for 1 min before their UV-visible and fluorescence spectra were recorded.

## RESULTS AND DISCUSSION

### Synthesis and characterisation

In this study we report the synthesis of the fluorescent monomer PePnUMA from the reaction between methylacryloyl chloride and 5-(perylene-3-yl)pent-4-yn-1-ol in the presence of  $\text{Et}_3\text{N}$ , using a procedure that was adapted from that reported by Zhang *et al.*<sup>51</sup> which had previously been reported for the synthesis of pyren-1-ylmethyl 2-methylprop-2-enoate (PyMA).<sup>51</sup> The  $^1\text{H}$  NMR and  $^{13}\text{C}$  NMR spectra of PePnUMA are depicted in Figs S1A, S1B in Appendix S1. The emission spectra of PyMA and PePnUMA are shown in Fig. S2.

The synthesis of a series of amphiphilic fluorescent copolymers was also undertaken using the random, free radical, copolymerisation of selected monomers in the presence of AIBN as an initiator and DMSO as solvent<sup>43</sup> (Scheme S1). Copolymerisation reactions, leading to CoP1-1, CoP1-2, CoP1-3, CoP2-1, CoP2-2

**Table 1.** Feeding masses of reactants used in the preparation of IPN hydrogels CoP2-3 and CoP1-1

IPNs	Acrylamide (g)	<i>N</i> -isopropylacrylamide (g)	PEG (g)	HEMA (g)	CoP2-3 (g)	CoP1-1 (g)
AH20	1.0	1.0	0.0	0.0	0.0	0.0
AH21	1.0	1.0	0.2	0.0	0.0	0.0
AH22	1.0	1.0	0.0	0.0	0.2	0.0
AH23	1.0	1.0	0.0	0.0	0.0	0.2
AH24	5.0	0.0	0.0	2.0	0.0	0.0
AH25	5.0	0.0	0.0	2.0	0.2	0.0
AH26	5.0	0.0	0.0	2.0	0.0	0.2

PEG, polyethylene glycol.

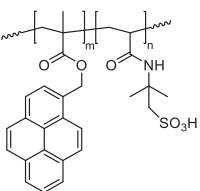
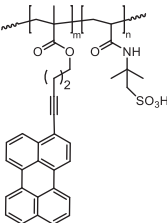
and CoP2-3, were performed using different monomer feed ratios as defined in Table 2. We observed that conducting these reactions in the presence of relatively low initiator concentrations (1 mol%) in DMF at 75 °C led to uniformly high degrees of monomer consumption (>75% for CoP1 and > 40% for CoP2). The feed mole ratios of AMPS, PyMA and PePnUMA, the structures of the copolymers and the reactant quantities are listed in Table 2.

The <sup>1</sup>H NMR spectra of CoP1-1 and CoP2-1 (Fig. 1) are similar to those reported for related AMPS–acrylate copolymers.<sup>47,48</sup> Importantly these spectra were devoid of the methylene protons at *ca* δ 5.6 and 6.2 ppm which are present in the starting materials, indicating full conversion of monomer to polymer. Moreover, the incorporation of two different monomer units into the backbone of these copolymers was confirmed by <sup>1</sup>H NMR, <sup>13</sup>C NMR and UV–visible spectroscopy, as illustrated in Figs 1, 2 and S3–S6. For CoP1-1 (Fig. 1(A)), the appearance of resonances between δ 8.1

and 8.6 ppm signifies the presence of the aromatic protons of the pyrene moiety, where the broadened appearance of these resonances when in a polymer matrix has been noted elsewhere.<sup>43,53–56</sup> In addition to the aromatic hydrogens this spectrum also possessed a broadened singlet (at δ 5.2 ppm), assigned to H<sub>b</sub>, which is also derived from the incorporation of PyMA. The resonance at δ 7.7 ppm is assigned to the amide N–H (H–NCO) which is derived from AMPS, as is the resonance at δ 2.9 ppm. The broadened resonance at δ 1.4 ppm corresponds to the methyl groups (–CH<sub>3</sub>) derived from AMPS and methacrylate moieties. A similar assignment for the <sup>1</sup>H NMR spectrum of CoP2-1 is shown in Fig. 1(B).

The ratio of PyMA and PePnUMA to AMPS in these materials could be calculated from their respective <sup>1</sup>H NMR spectra. This is based upon the integration of the methylene protons H<sub>h</sub>, next to the sulfonic acid residue in AMPS and PyMA monomers in CoP1. It was found that the copolymer compositions are close to

**Table 2.** Structures of copolymers, reactant quantities, yield and molecular weight distributions of the synthesised copolymers

Structure/symbol	Feed monomer ratios				Composition (mol%)			
	Yield	PyMA	PePnUMA	AMPS	PyMA	PePnUMA	<i>M<sub>w</sub></i> / <i>M<sub>n</sub></i> <sup>c</sup>	<i>D</i>
 CoP1								
 CoP2								
CoP1-1	80%	1.0	0.0	5.0	1:5 <sup>a</sup> , (14.5) <sup>b</sup>	None added	10 300/5900	1.7
CoP1-2	77%	1.0	0.0	10.0	1:9 <sup>a</sup> , (6.1) <sup>b</sup>	None added	10 300/5200	1.9
CoP1-3	83%	1.0	0.0	30.0	1:22 <sup>a</sup> , (1.5) <sup>b</sup>	None added	24 000/12900	1.8
CoP2-1	43%	0.0	1.0	10.0	None added	(9.2) <sup>b</sup>	10 200/3500	2.9
CoP2-2	41%	0.0	1.0	20.0	None added	(3.6) <sup>b</sup>	8500/5700	1.4
CoP2-3	42%	0.0	1.0	30.0	None added	(2.4) <sup>b</sup>	9000/5000	1.7

*D* is the ratio of the weight average molecular weight *M<sub>w</sub>* to the number average molecular weight *M<sub>n</sub>*.

<sup>a</sup> Determined by <sup>1</sup>H NMR analysis (Figs 1(a) and S3).

<sup>b</sup> Determined by UV–visible spectroscopy (mol%).

<sup>c</sup> Determined by GPC analysis.

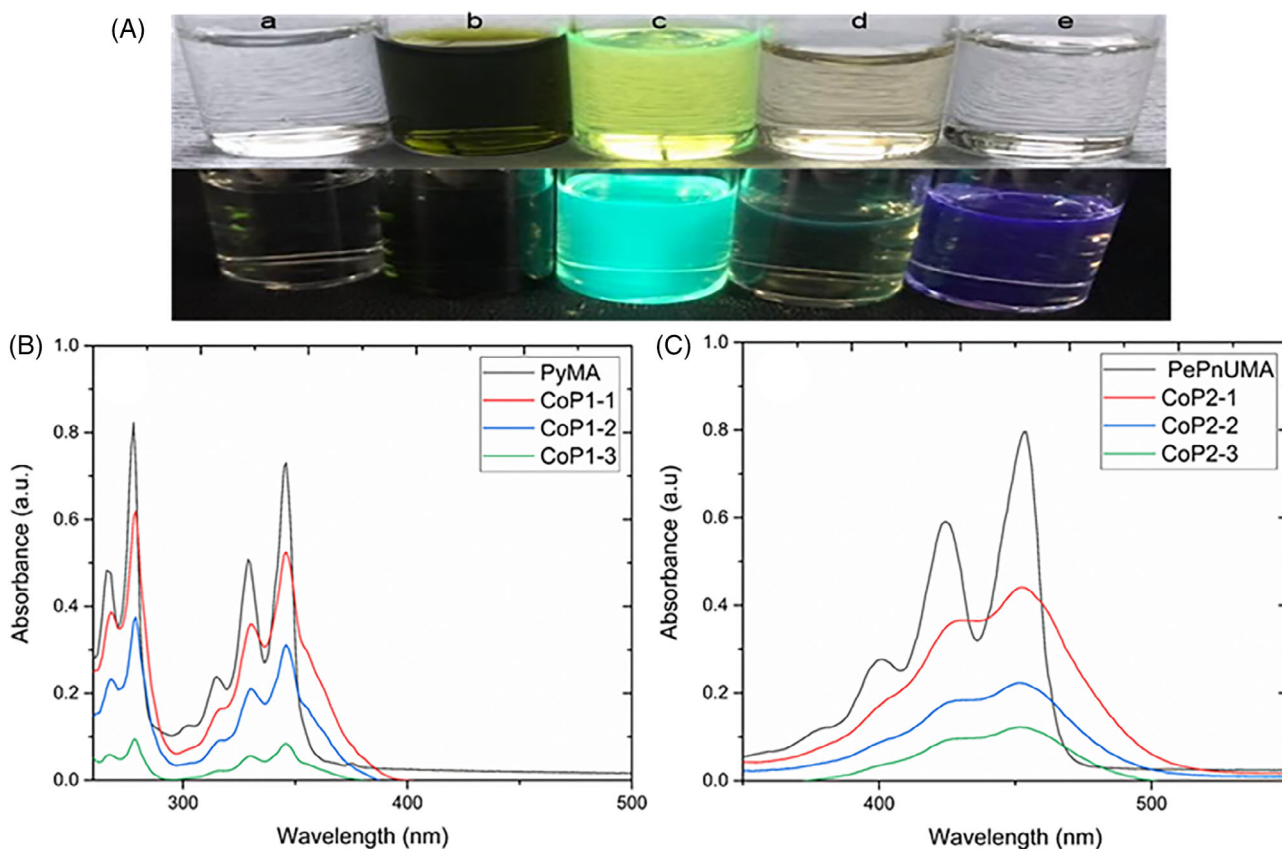


**Figure 2.** (A) Solutions of (a) AMPS, (b) CoP2-3, (c) PePnUMA, (d) CoP1-1 and (e) PyMA in DI water ( $1 \text{ mg mL}^{-1}$ ,  $2.8 \text{ nmol L}^{-1}$ ,  $3.0 \text{ nmol L}^{-1}$  and  $1.3 \times 10^{-2} \text{ mmol L}^{-1}$ ,  $1 \text{ mg mL}^{-1}$  respectively) under ambient lighting (top) and under UV illumination at 365 nm (bottom). (B) The UV-visible absorption spectra for solutions of PyMA and CoP1 copolymers. (C) The UV-visible absorption spectra for PePnUMA and CoP2 copolymers in DI water.

the same feed ratio of monomers in the copolymerisation process. A similar analysis for CoP-2 was not possible due to the overlapping resonances from the alkyl moieties derived from AMPS and PePnUMA.

The  $^{13}\text{C}$  NMR spectra of CoP1 and CoP2 are presented in Figs S5 and S6. These spectra indicate the presence of the ester carbonyl ( $174 \text{ ppm}$ ), methyl ( $-\text{CH}_3$ ,  $27 \text{ ppm}$ ) and methine ( $-\text{CH}$ ,  $60 \text{ ppm}$ ) groups. All the remaining methylene resonances ( $-\text{CH}_2$ ) appear between 34 and 58 ppm while the aromatic resonances lie between 124 and 132 ppm. The IR spectra of these copolymers are also in accord with their structure and display characteristic absorptions at  $3300 \text{ cm}^{-1}$  (N-H and O-H),  $3076 \text{ cm}^{-1}$  (Ar C-H),  $2978$  and  $2942 \text{ cm}^{-1}$  (C-H),  $1698$  and  $1748 \text{ cm}^{-1}$  (C=O of amide and ester respectively),  $1368 \text{ cm}^{-1}$  (C-H of  $\text{CH}_3$  group),  $1298 \text{ cm}^{-1}$  (Ar C=C),  $1215 \text{ cm}^{-1}$  (C-N) and  $1138 \text{ cm}^{-1}$  (C-O), while the two bands at around  $1160$  and  $1040 \text{ cm}^{-1}$  can be assigned to the asymmetric and symmetric  $\text{SO}_2$  stretching frequencies of the sulfonic acid group.<sup>48,52</sup> The UV-visible spectra of all of the copolymers made in this study ( $3.0 \text{ nmol L}^{-1}$  in DMSO) are presented in Fig. 2. In addition the UV-visible spectra of copolymers CoP1 and CoP2 were also used to calculate the pyrene and perylene content of each polymer by application of the Beer-Lambert law.<sup>57</sup> (The molar absorbance coefficients used in the calculations were as follows: 1-pyrenemethanol,  $\lambda_{\text{em}}$  of  $340 \text{ nm}$ ,  $28\,000 \text{ mol}^{-1} \text{ cm}^{-1}$  in DMSO; and 5-(perylene-3-yl)pent-4-yn-1-ol,  $\lambda_{\text{em}}$  of  $420 \text{ nm}$ ,  $29\,823 \text{ mol}^{-1} \text{ cm}^{-1}$  in DMSO.)

The calculated ratios are in satisfactory agreement with those determined by  $^1\text{H}$  NMR spectroscopy as shown in Table 2.

Figure 2(B) shows the UV-visible spectra of PyMA, CoP1-1, CoP1-2 and CoP1-3 in DI water ( $2.8 \text{ nmol L}^{-1}$ ). The four characteristic absorbance bands in the range 278–345 nm, corresponding to  $S_0 \rightarrow S_3$ ,  $S_0 \rightarrow S_4$ ,  $S_0 \rightarrow S_2$  and  $S_0 \rightarrow S_1$  transitions, are similar to those previously reported<sup>58–60</sup> for PyMA and the corresponding copolymer which indicates the incorporation of the pyrene unit into these new copolymers. In addition Fig. 2(C) shows the three characteristic absorbance maxima in the range of 400–451 nm which can be assigned to  $S_0 \rightarrow S_2$ ,  $S_0 \rightarrow S_1$  and  $S_0 \rightarrow S_0$  transitions of PePnUMA, observations that are in keeping with Ryder's analysis.<sup>61</sup>

### Photophysical and fluorescence quenching studies

The effect of adding CoP2-3 ( $2 \text{ mL}$ ,  $0.01 \text{ mmol L}^{-1}$ ) to aqueous solutions of metal ions was investigated by UV-visible and fluorescence spectroscopy. There is no significant change in the UV-visible spectra of CoP2-3 following the addition of  $\text{Co}^{2+}$ ,  $\text{Hg}^{2+}$ ,  $\text{Pb}^{2+}$ ,  $\text{K}^+$ ,  $\text{Na}^+$  and  $\text{Mg}^{2+}$  as shown in Fig. 3(A) although the intensity of the absorption at  $450 \text{ nm}$  was sensitive to the addition of  $\text{Cu}^{2+}$  and  $\text{Ni}^{2+}$  as shown in Fig. 3(A) and S7(D) in Appendix S7. Closer analysis revealed that the absorption intensity of CoP2-3 ( $0.01 \text{ mmol L}^{-1}$ ) at  $450 \text{ nm}$  versus  $\text{Cu}^{2+}$  concentrations  $0.0$ – $7.1 \text{ }\mu\text{mol L}^{-1}$  results in a linear dependence ( $R^2 = 0.98$ ) equating to an absorption coefficient of  $221\,800 \text{ L mol}^{-1} \text{ cm}^{-1}$ . The molar

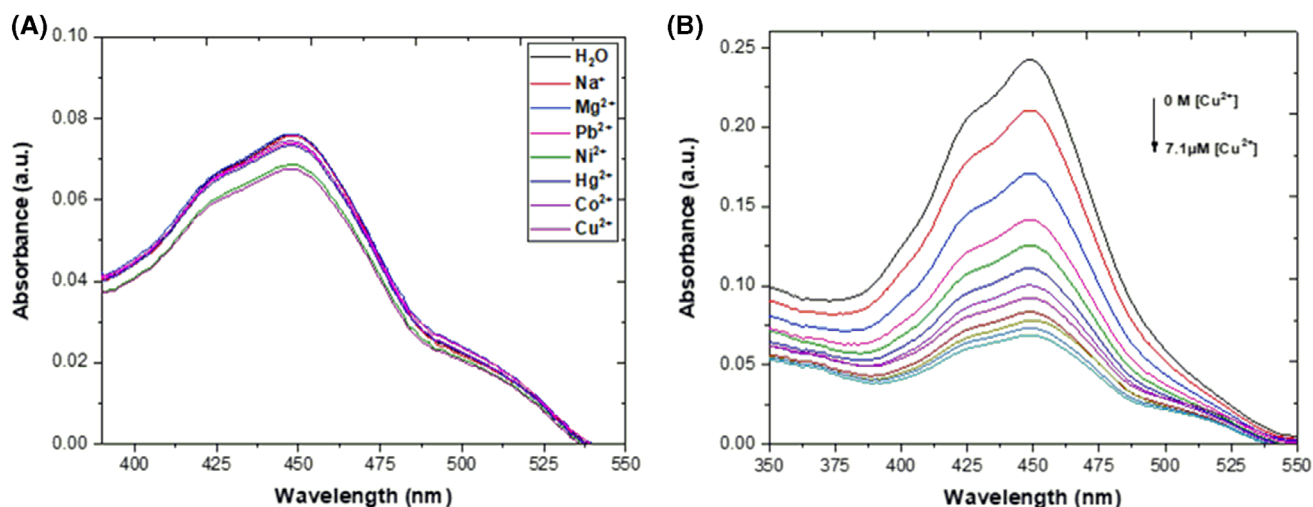


**Figure 3.** Absorption spectra for the titration of (A) CoP2-3 with 2.5 equiv. of metal ions in DI water; (B) CoP2-3 with different concentrations of Cu<sup>2+</sup> solution (0.0–7.1 μmol L<sup>-1</sup>).

absorption coefficient of CoP2-3 when recorded in the presence of a series of metal ions is presented in Table 3. The UV–visible spectra of CoP2-3 in the presence of a series of metal ions are given in Fig. S7.

In addition the fluorescence spectra of CoP2-3 were also recorded in the absence and presence of metal ions in order to determine whether there is any selectivity to specific metals in the study in the fluorescence quenching of the polymer solution under these conditions. Initially the fluorescence emission of CoP2-3 was recorded in DI water (0.01 mmol L<sup>-1</sup>), at pH 6.8, where it was found to have a broad emission band from 390 to 650 nm, with a maximum at 465 nm, when irradiated at 420 nm. The emission spectrum of this solution was then recorded in the presence of varying quantities of Co<sup>2+</sup> (0.0–2.5 equiv.) as shown in Fig. 4(A). The fluorescence spectrum of CoP2-3 (concentration 0.0–7.1 μmol L<sup>-1</sup>) was also measured in the presence of Co<sup>2+</sup> (0.48–7.1 μmol L<sup>-1</sup>). These measurements indicated that the intensity of the emission decreased by 10% at a Co<sup>2+</sup> concentration of 0.48 μmol L<sup>-1</sup> (0.1 equiv.) while it reached 80.99% from the original value with Co<sup>2+</sup> of 7.1 μmol L<sup>-1</sup>, 2.5 equiv. (Fig. 4(B)). There was no shift in wavelength of the maximum fluorescence peak.

A Stern–Volmer plot (Fig. 4(C)) of  $F_0/F$  (quenching efficiency) versus [Co<sup>2+</sup>] shows a linear relationship ( $R^2 = 0.955$ ) over a limited, low concentration range of Co<sup>2+</sup> as defined by

$$\frac{F_0}{F} = 1 + K_{SV}[Q] \quad (4)$$

where  $F_0$  and  $F$  are the fluorescence intensities of the copolymer solution in the absence and presence of the metal ion respectively;  $K_{SV}$  is the Stern–Volmer constant and  $[Q]$  is the metal ion concentration.

These data suggest that static fluorescence quenching may be the dominant quenching mechanism at low [Co<sup>2+</sup>] but the upward deviation that is observed above 4 μmol L<sup>-1</sup>, which can be fitted to a linear relationship, suggests that the onset of other quenching processes (e.g. both dynamic and static quenching) may be operative.<sup>58–60,62</sup> A static fluorescence quenching mechanism involves the formation of a non-fluorescent complex due to the interaction between perylene, fluorophore and the metal ion, which take place in the ground state of perylene. The concentration of metal ion, quencher and the formation constant of this complex govern the quenching efficiency. Alternatively, in the case of a dynamic quenching mechanism, the metal ion interacts with the fluorophore molecule during the lifetime of the excited state of the fluorophore molecule. Here, the lifetime of the excited state of the fluorophore, the viscosity of the solution and the concentration of the metal ion all contribute to quenching efficiency. It is clear that all the metal ions studied quenched the

**Table 3.** Shows some UV–visible and fluorescence responses of CoP2-3 to metal ions

Metal ions	From UV–visible spectroscopy		From fluorescence			
	Molar absorption coefficient (L mol <sup>-1</sup> cm <sup>-1</sup> )	$R^2$	$K_{SV} \times 10^{-6}$ (L mol <sup>-1</sup> )	$R^2$	LOD (μmol L <sup>-1</sup> )	LOQ (μmol L <sup>-1</sup> )
Co <sup>2+</sup>	227 120	0.992	0.18	0.996	0.69	2.29
Cu <sup>2+</sup>	223 034	0.987	0.15	0.998	0.68	2.27
Ni <sup>2+</sup>	236 110	0.995	0.11	0.997	0.72	2.40
Hg <sup>2+</sup>	227 392	0.991	0.13	0.999	0.77	2.58
Pb <sup>2+</sup>	231 007	0.994	0.11	0.998	0.77	2.55
Mg <sup>2+</sup>	224 870	0.990	0.10	0.998	0.83	2.76
Na <sup>+</sup>	228 443	0.992	0.09	0.999	0.87	2.91

Metal ion concentration 0–7.1 μmol L<sup>-1</sup> in DI water at room temperature (pH 6.8).

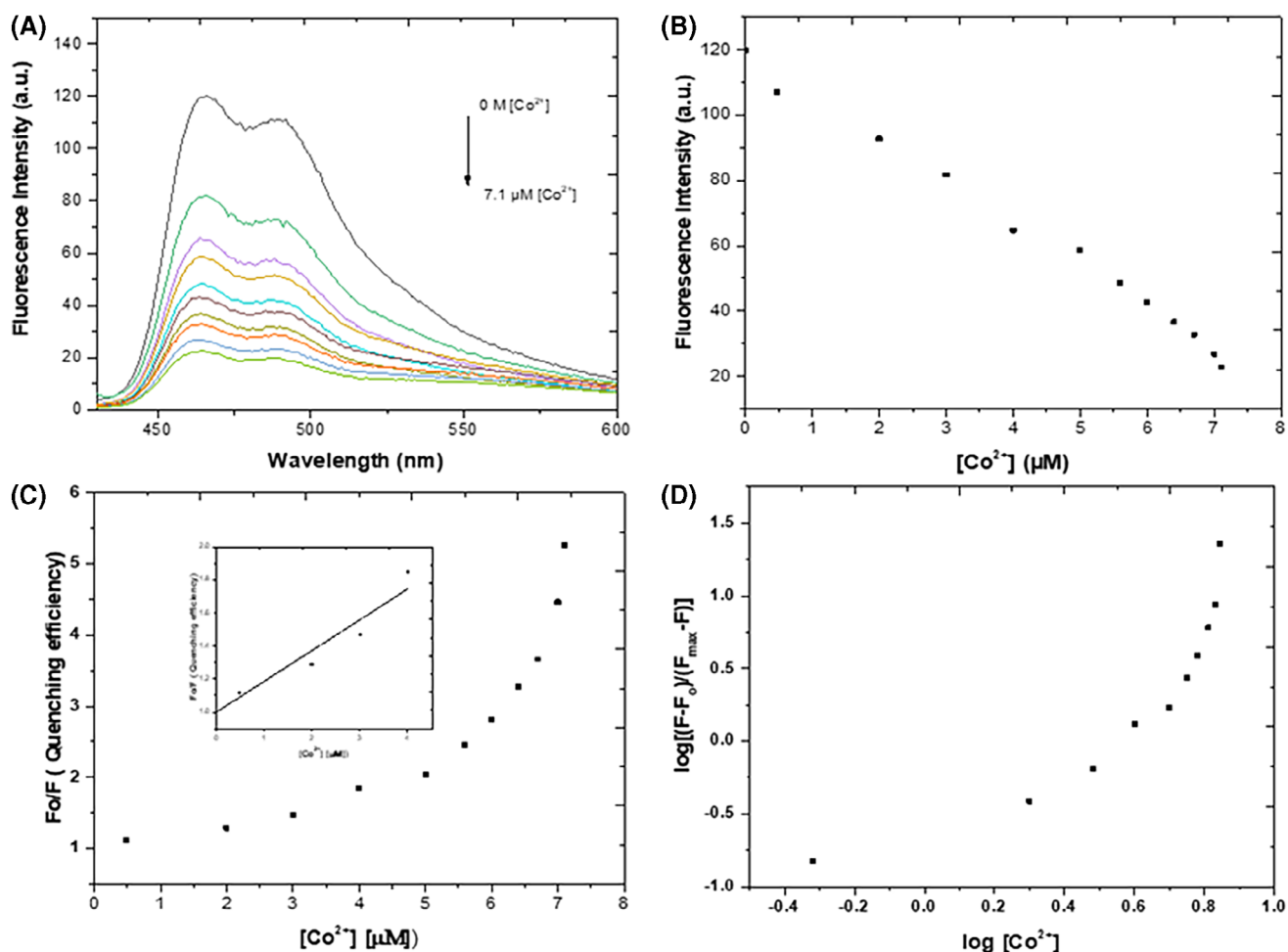


**Figure 4.** (A) Fluorescence titration spectra of CoP2-3 with various concentrations of aqueous Co<sup>2+</sup> solution (0.0–7.1 μmol L<sup>-1</sup>, pH 6.8); (B) the fluorescence intensity at 465 nm with various concentrations of Co<sup>2+</sup>; (C) the quenching efficiency with various concentrations of Co<sup>2+</sup>; the inset shows Stern–Volmer plots for fluorescence quenching by the Co<sup>2+</sup>; and (D) the plot of  $\log[(F - F_0)/(F_{\max} - F)]$  versus  $\log[\text{Co}^{2+}]$  for the titration of CoP2-3 with Co<sup>2+</sup> (in DI water at pH 6.8).

fluorescence of the polyaromatic-hydrocarbon-containing copolymers, a process which is more efficient in the presence of Co<sup>2+</sup> and Cu<sup>2+</sup>. This result can be explained by the paramagnetic properties of Co<sup>2+</sup> (d<sup>7</sup>) and Cu<sup>2+</sup> (d<sup>9</sup>); both metals have unpaired d-electrons which quench effectively both singlet and triplet states of the copolymer, a phenomenon that has been noted previously.<sup>63,64</sup>

The quenching experiments that were conducted at low Co<sup>2+</sup> concentrations enabled the calculation of the quenching constant ( $K_{SV}$ ), which in this case had a value of  $1.86 \times 10^{-7} \text{ L mol}^{-1}$ . The quenching constants for CoP2-3 in the presence a series of metal ions were also calculated in a similar manner, as listed in Table 3.

The fluorescence quenching of CoP2-3 by the addition of metal ions suggests that there is a fluorophore-quencher complex that has a different absorption spectrum,<sup>65</sup> a process which is supported by the observed overlap in the emission and absorption spectra of CoP2-3 recorded in the presence of Co<sup>2+</sup>, as depicted in Fig. 5.

There was no noticeable change or decrease in the fluorescence lifetimes of CoP2-3 with the metal ions used in this study. This is to be compared with the values obtained for CoP2-3 alone ( $\tau_1 = 2.2 \text{ ns}$  and  $\tau_2 = 5.1 \text{ ns}$ ) as shown in Fig. S8. These observations are in consonance with a static quenching mechanism<sup>66,67</sup> via complexation of CoP2-3 with metal ions (Table S1).

Unfortunately Benesi–Hildebrand plots (i.e. plots of  $\log(F - F_0)/(F_{\max} - F)$  versus  $\log[Q]$ ) of CoP2-3 for a variety of metals proved to be nonlinear, as shown for Cu<sup>2+</sup> (Fig. 4(D)), and association constants between the polymer and metal ions could not therefore be determined.<sup>68</sup> The fluorescence quenching efficiencies ( $F_0/F$ ) for a range of metal ions (Na<sup>+</sup>, Mg<sup>2+</sup>, Hg<sup>2+</sup>, Pb<sup>2+</sup>, Ni<sup>2+</sup> and Cu<sup>2+</sup>) of CoP2-3 are also tabulated in Fig. 6. From these data it can be seen that both the Cu<sup>2+</sup> and Co<sup>2+</sup> ions exhibited high quenching efficiency compared to Ni<sup>2+</sup>, while a small quenching effect was observed for Mg<sup>2+</sup> and Na<sup>+</sup> ions.<sup>69</sup> Fluorescence data of all the metal ions studied in this work can be found in Figs S9–S15.

The IR spectra of CoP2-3 are shown in Fig. 7 in DI water. Most noticeably the IR absorptions which were assigned<sup>48,52</sup> to the S–O group (1040, 1160 and 1180 cm<sup>-1</sup>) disappeared upon introduction of the metal ions but there was no shift for the amide carbonyl absorption at 1640 cm<sup>-1</sup>. This behaviour suggests that the metal ions interact with the sulfonic acid moiety in the polymer rather than the amide group upon mixing.<sup>70</sup>

Binding of metal ions to CoP2-3 also appears to be pH dependent. We note, for example, that at pH 12 there is no appreciable loss of fluorescence when metal ions are mixed with CoP2-3 (Fig. 8). This suggests that at high pH the sulfonic acid moieties associated with the AMPS unit are fully ionized and are associated



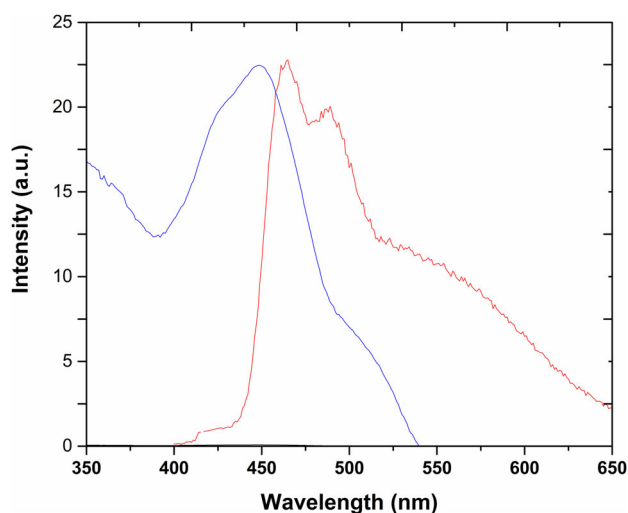


**Figure 5.** Overlap of the emission and absorption spectra for CoP2-3 in the presence of  $\text{Co}^{2+}$  (2.5 equiv. in DI water).

with the sodium counterions.<sup>71</sup> In this situation intramolecular self-association and excimer formation between perylene units becomes important, as indicated by the appearance of the broad and structureless band centred at 542 nm, as shown in Fig. 8.

The limit of detection (LOD) and limit of quantitation (LOQ) of CoP2-3 were determined for all metal ions using a plot of fluorescence intensity *versus* concentration of metal ion. LOD and LOQ were calculated from the equations<sup>72,73</sup>

$$\text{LOD} = 3\sigma/k(5)$$

$$\text{LOQ} = 10\sigma/k(6)$$

The standard deviation of the maximum fluorescence intensity ( $\sigma$ ) of CoP2-3 ( $0.01 \text{ mmol}^{-1}$  in DI water) was measured more than six times and  $k$  is the slope of the relationship between fluorescence intensity and concentration of metal ions are shown in Table 3.

The LOD depends heavily on the concentration of metal ions and their electrostatic interactions with the polar functionality that is embedded within the polymer.<sup>74</sup> Measurement of the LOD in this series was carried out using CoP2-3 which has ionised sulfonic acid residues and excellent fluorescence characteristics.<sup>74</sup>

The photophysical studies of CoP1-2 and CoP2-3, namely their efficient fluorescence quenching in the presence of heavy metal cations, encouraged us to incorporate these materials into hydrogels for use in heavy metal detoxification. These studies were performed on a series of hydrogels (AH20–AH26, where AH20, AH21 and AH24 are controls) from CoP1-2 and CoP2-3 with diverse monomers.

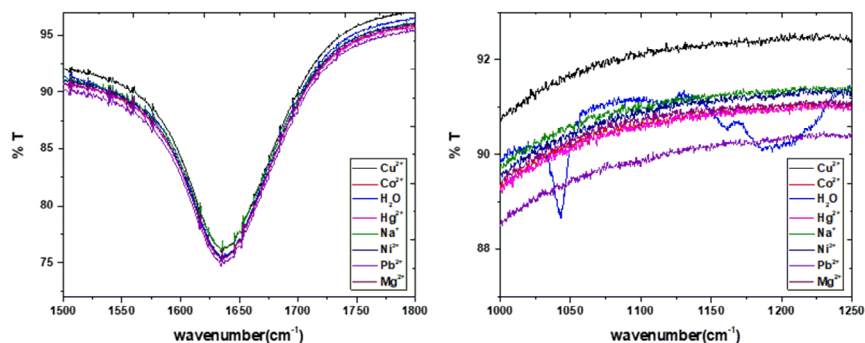


**Figure 7.** IR spectra of CoP2-3 solution with and without metal ions.

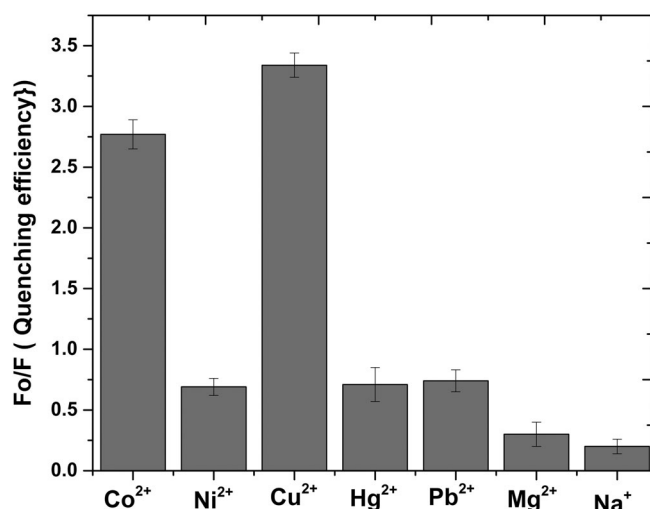


**Figure 6.** Histogram comparing the quenching efficiency of CoP2-3 towards different metal ions (2.5 equiv.) in DI water (graph normalized with respect to water dilution).

Figure 9 shows the swelling ratio of the prepared hydrogels in metal ion solution. It is noticeable that AH20–AH23 have higher swelling ratios than AH24–AH26 due to the presence of HEMA in the AH24–AH26 compositions. Interestingly, the presence of CoP1-1 in AH23 gives higher values of the swelling ratios in all metal ion solutions under study than the controls (AH20, AH21). On the other hand, the presence of CoP2-3 in AH22 gave higher values of the swelling ratio in only copper and lead ion solutions, whereas it gave close values in cobalt and nickel ion solution compared with AH20 and AH21, which contain acrylamide and *N*-isopropylacrylamide only. The swelling ratios for AH25 and AH26, which contain CoP2-3 and CoP1-1 respectively, are very close to their control, AH24.

Figure 9(B) shows the ability of these hydrogels to absorb metal ions. These results indicate that the acrylamide–*N*-isopropylacrylamide hydrogels (AH20 and AH21) do not have any ability to absorb cobalt and nickel ions while the acrylamide–CoP2-3 hydrogel (AH22) could absorb up to 23% of  $\text{Ni}^{2+}$  and only 5% of  $\text{Co}^{2+}$ . The acrylamide–CoP1-1 hydrogel (AH23) was able to absorb more than 68%  $\text{Co}^{2+}$  and 67%  $\text{Ni}^{2+}$ , while AH22 and AH23 exhibited excellent efficiency in the uptake of copper and lead ions compared with AH20 and AH21 (control). Replacing *N*-isopropylacrylamide with HEMA in the hydrogel tends to result in a lower swelling ratio of the hydrogel. Hydrogel AH24 appears to be a particularly selective sequester of  $\text{Ni}^{2+}$  and  $\text{Pb}^{2+}$  compared to  $\text{Cu}^{2+}$  and  $\text{Co}^{2+}$  ions,

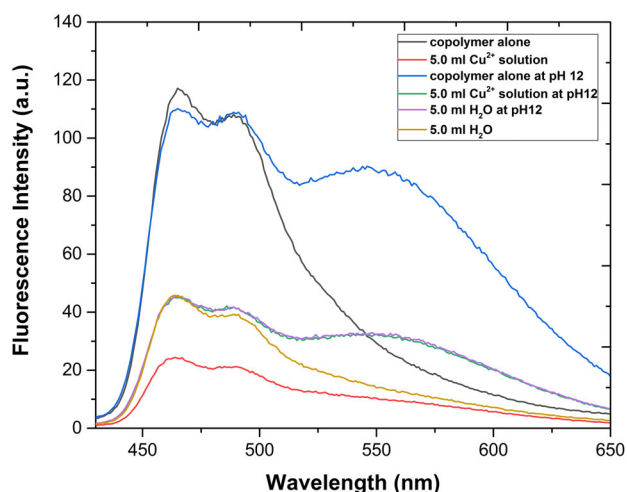


**Figure 8.** Fluorescence spectra for CoP2-3 with and without Cu<sup>2+</sup> (2.5 equiv., pH 6.8 and 12).

an outcome that may plausibly be attributed to the additional binding site proffered by the hydroxyl moiety present in HEMA.

Incorporation of CoP1-1 and CoP2-3 into the HEMA–acrylamide hydrogels AH25 and AH26 resulted in decreased ability for Ni<sup>2+</sup> and Cu<sup>2+</sup> sequestration but an increased affinity for Co<sup>2+</sup> uptake, whereas the uptake efficiency for Pb<sup>2+</sup> is the same for AH24, AH25 and AH26. We attribute this observation to the presence of the sulfonic acid group (as in CoP1-1 and CoP2-3) where the inclusion of CoP1-1, CoP2-3 and HEMA in the hydrogel matrix (Fig. 9(C)) results in irreversible entrapment of metal ions.

#### DSC and TGA measurements

The thermal properties of the prepared copolymers were investigated by TGA and DSC; 4–5 mg of each copolymer sample was measured under N<sub>2</sub> gas between 20 and 800 °C at a constant heating rate of 10 °C min<sup>-1</sup>. Analysis of the TGA thermograms afforded the initial decomposition temperature (*T<sub>i</sub>*), the temperature of the final decomposition (*T<sub>f</sub>*), the degree of decomposition

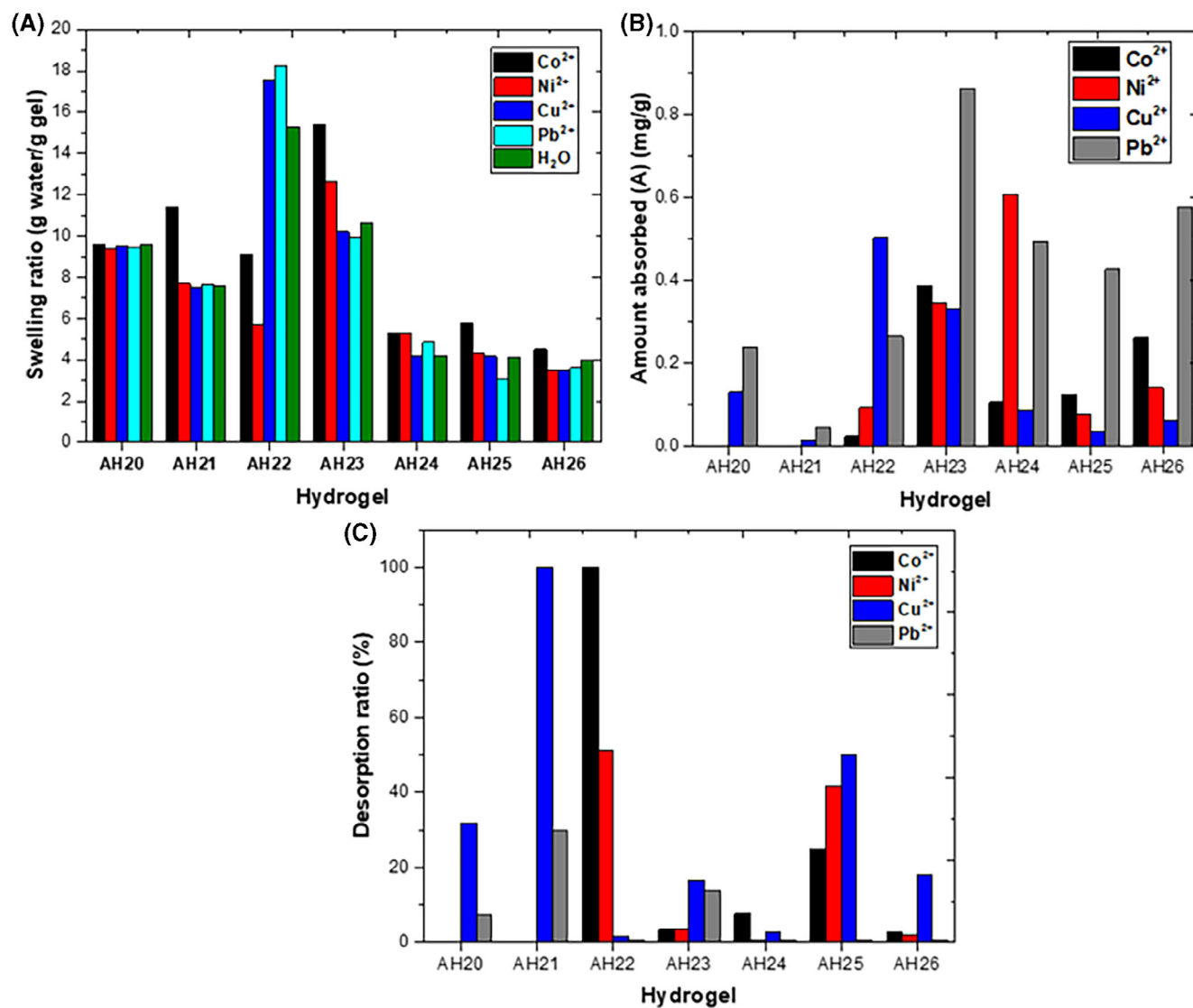


**Figure 9.** (A) The swelling ratio of all prepared hydrogels in metal ion solution and DI water; (B) the amount of metal ions absorbed by the prepared hydrogels; and (C) the desorption ratio of metal ions from hydrogels in DI water.

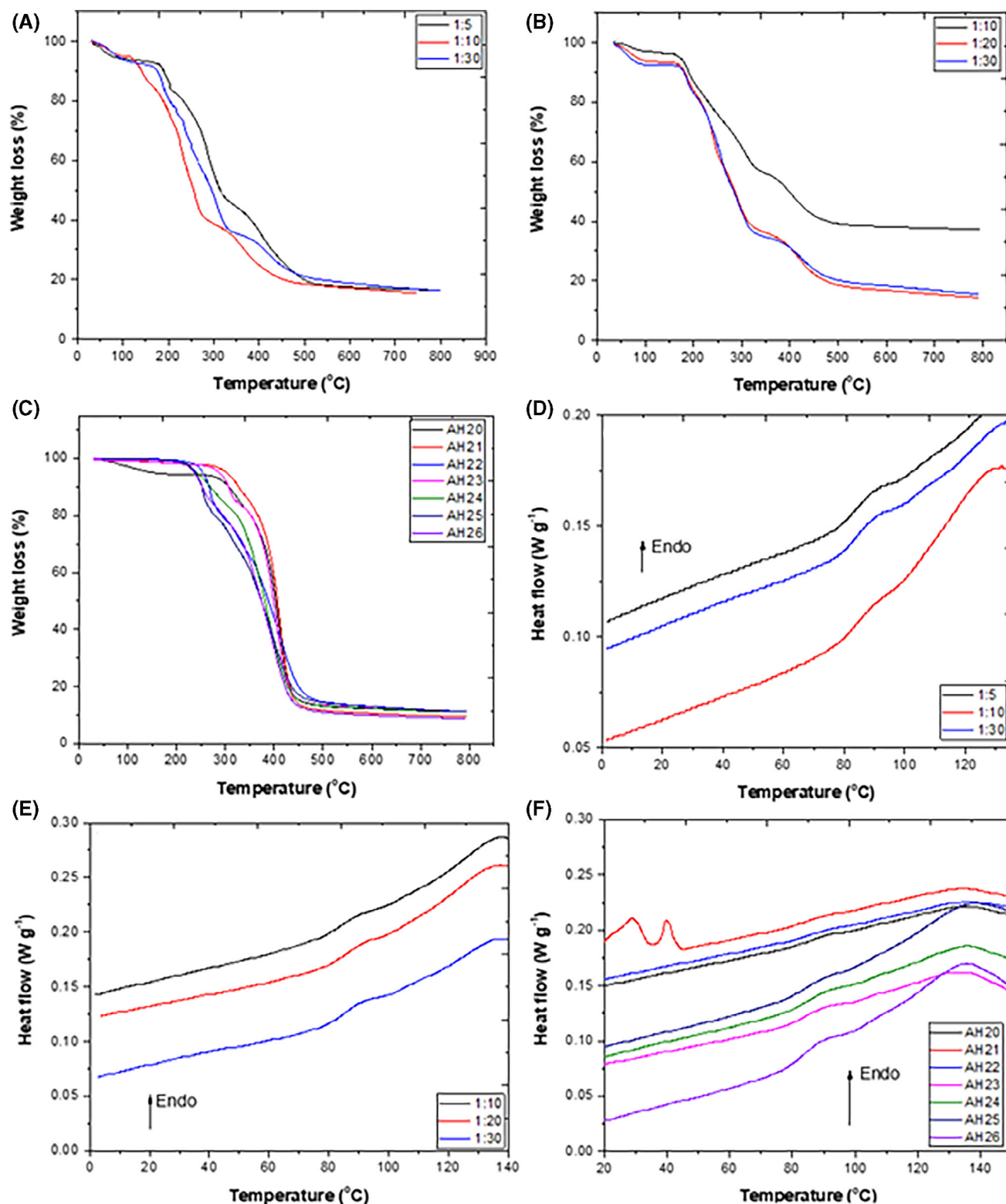


**Figure 10.** TGA thermograms of (A) CoP1; (B) CoP2; (C) AH20–AH26 hydrogels. (D) DSC thermogram of CoP1; (E) DSC thermogram CoP2; (F) DSC thermograms of all the hydrogels prepared in this study.

temperature at 50% loss of sample weight ( $T_{50\%}$ ) and char content at 800 °C values that are listed in Table S2. The rate of decomposition was calculated from the slope of the degradation curve between 20% and 80% weight loss.

Figures 10(A) and 10(B) show the TGA thermograms for pyrene copolymers and perylene copolymers respectively where the first decomposition stage can be attributed to scission of the sulfonic acid residue.<sup>75,76</sup>

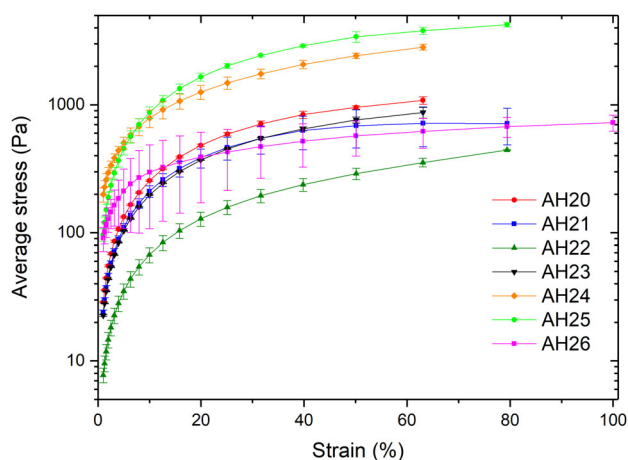


**Figure 11.** Stress–strain curves of AH20–AH26.

It is clear that the first initial decomposition temperature is higher for CoP1-1 and CoP2-1 and that these systems have a greater proportion of pyrene or perylene monomers in the copolymer composition compared to CoP1-3 and CoP2-3. The second stage is due to decomposition of copolymer chains while the third stage can be attributed to loss of the aromatic residues. The rate of the second decomposition stage is higher for all these copolymers while it is lower for the third stage of the decomposition due to loss of the stable aromatic residues. The char content varied between 14 and 16 wt% except for CoP2-3 as CoP2-3 exhibited a very high stability compared to the other prepared copolymers and had a 37% char content.

Figure 10(C) shows the TGA thermograms of the prepared hydrogels AH20–AH26. Control hydrogels AH20, AH21 and AH24 were found to decompose in one stage while the hydrogels containing the pyrene and perylene copolymers show a broader decomposition range to higher temperatures. The initial decomposition temperature is higher for the hydrogels that incorporate CoP1-1 into their structure and this can be attributed to lower

steric hindrance with a pyrene core compared with a perylene core.<sup>77</sup> Tables S2 and S3 show all thermal property data for the prepared copolymers and hydrogels respectively.

From the DSC thermograms (Fig. 10(D)) we note glass transition temperatures of 76.0–77.8 °C for CoP1 and 76.4–79.7 °C for CoP2. Higher glass transition temperatures were observed for those hydrogels that contained lower ratios of pyrene and perylene sub-units. This can be attributed to steric hindrance between the pyrene and perylene side chains.<sup>77</sup> The glass transition of hydrogels AH20–AH26 (Fig. 10(F)) was obtained between 75.3–79.4 °C. These results assume that the incorporation of pyrene and perylene copolymers did not significantly change the glass transition temperature of the prepared hydrogels and this may be due to the low content of the pyrene and perylene copolymers. The hydrogel that incorporated polyethylene glycol (AH21) exhibited two semi-crystalline peaks<sup>78</sup> between 30 °C and 45 °C.

### Stress–strain analysis

The stress–strain analysis of gels AH20–AH26 demonstrates pseudo-plastic (shear thinning) behaviour over the strain range examined<sup>32,79,80</sup> (Fig. 11). Gels AH24 and AH25 were noted to have a region of elastic behaviour over a larger range than the other gels examined (AH20–AH23 and AH26), which showed a larger region of plastic deformation. These gels may be considered to be suitably robust and stable under these test conditions as no material failure occurred, which would be indicated by a sudden and abrupt decline in measured stress. The increased angle of the curves of the gels AH24 and AH25 suggest that these gels are stiffer than the others examined, a point evident during manual handling as these gels were more robust and less fragile, allowing increased ease of use in contact applications. Complementary data for further rheological characterisation including the crossover point for gels, the complex viscosity ( $\eta^*$ ) as a function of frequency,  $G'$  and  $G''$  as a function of frequency,  $\tan \delta$  as a function of frequency (L), low  $\tan \delta$  region (R) are summarised in Appendix S1 (Table S4 and Figs S16–S19).

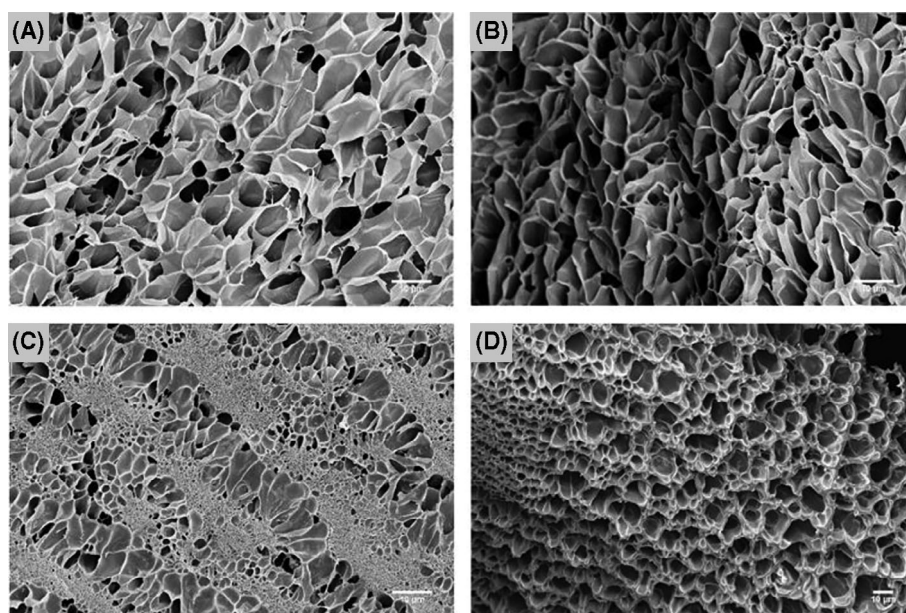


**Figure 12.** SEM images of AH22, AH23, AH25 and AH26.

**Table 4.** Observed pore size range and volume fraction of examined hydrogels

Gel	Minimum observed pore size ( $\mu\text{m}$ )	Maximum observed pore size ( $\mu\text{m}$ )	Solid fraction (%)
AH20	0.08	10.36	60.0
AH21	0.06	19.50	N/A
AH22	0.06	20.98	52.0
AH23	0.34	22.21	47.0
AH24	0.06	20.56	54.0
AH25	0.01	14.42	41.0
AH26	1.12	17.01	63.0

The  $G'$  and  $G''$  data obtained (included in the Supporting information) confirm that the samples (with the exception of AH24 and AH26) exhibit typical gel-like behaviour as  $G'$  is dominant over  $G''$ . Samples AH24 and AH26, however, do not conform to the typical rheological behaviour of stronger hydrogels at lower strain and thus are more typical of weak gels with poor mechanical properties.<sup>81,82</sup>

A direct comparison between the gels described here and literature precedent AMPS-based hydrogels is, in many cases, not possible due to the absence of rheological investigation and/or reporting in many published studies; many publications also differ significantly in the form of the rheological investigations performed due to the intended method of gel use and a directed interest into the initial gelation mechanism of the gels examined.<sup>83</sup> Temperature sweeps were not performed in this instance due to the intended use of these gels at ambient temperature.

### Surface morphologies of hydrogels

The formulations of the prepared gels were examined by SEM measurements (Fig. 12) where it was found that pore sizes ranged from 0.01  $\mu\text{m}$  to 22.21  $\mu\text{m}$  across the range of samples. Gel solid fractions were observed to range from 41% to 60% of gel total volume in a continuous network.

Table 4 lists the range of pore sizes and solid fractions measured from these SEM images. Of the gels examined AH25 possessed the smallest pore sizes whereas AH23 had both the largest minimum and maximum pore sizes. The volume fractions observed in these samples demonstrate an open, hydrated, pore structure which we presume to be essential for the immobilisation and retention of metal ions adsorbed from solution.

### CONCLUSION

In this work we have developed an operationally simple synthesis of water soluble, amphiphilic pyrene- and perylene-containing fluorescent materials derived from the copolymerisation of 1-pyrenemethyl methacrylate or 5-(perylene-3-yl)pent-4-yn-1-yl methacrylates with commercially available AMPS. There are no literature reports of related perylene copolymers of this type. The UV-visible absorption and fluorescence spectra of these materials were measured in order to examine the interaction of the polyaromatic hydrocarbon residues with each other within the polymer matrix. These copolymers undergo fluorescence quenching in the presence of metal ions (e.g.  $\text{Co}^{2+}$  and  $\text{Cu}^{2+}$ ,  $\text{Ni}^{2+}$ ,  $\text{Hg}^{2+}$ ,  $\text{Pb}^{2+}$ ), a process that follows Stern–Volmer behaviour at low metal concentrations (0.0–7.1  $\mu\text{mol L}^{-1}$ ), which is indicative of a static quenching mechanism. This sequestration behaviour is also characterised by nonlinear Benesi–Hildebrand plots which suggest that the binding between the metal centre and sulfonic acid residues in the polymer has an ill-defined stoichiometry. The

LOD and LOQ for  $\text{Co}^{2+}$ ,  $\text{Cu}^{2+}$ ,  $\text{Ni}^{2+}$  and  $\text{Hg}^{2+}$  were found to lie between 0.69 and 0.87 and between 2.27 and 2.91  $\mu\text{mol L}^{-1}$  respectively.

Semi-IPN hydrogels were fabricated by the incorporation of these copolymers into acrylamide, *N*-isopropylacrylamide and hydroxyethylmethacrylate matrices. Hydrogels incorporating pyrene and perylene copolymers showed increased divalent metal ion uptake at neutral pH, particularly  $\text{Pb}^{2+}$  where up to 99% adsorption was achieved with AH26. Desorption studies, at neutral pH, indicate irreversible capture of the metal ions by the hydrogel. The copolymers and hydrogels prepared in this study have good chemical and thermal stability which makes them promising candidates for multiple applications, especially for the detection and removal of heavy metals from aqueous environments at neutral pH.

### AUTHOR CONTRIBUTIONS

AH, SY and PQ conceived and developed the overall research plan and designed the research. AA, MA and AH conducted the synthetic work; JM and CB conducted the SEM and rheological characterization; AW and LN conducted the lifetime measurements. All authors contributed to the writing of the manuscript and have approved its submission.

### CONFLICT OF INTEREST

There are no conflicts to declare.

### ACKNOWLEDGEMENT

The University of Manchester thanks the EPSRC (EP/K039547/1) for the provision of Bruker NMR spectrometers. A. A. Alwattar gratefully acknowledges the Iraqi Ministry of Higher Education and Scientific Research (MOHER) and the University of Basrah (Chemistry Department) for the provision of a research scholarship. M. Alshareef thanks the Ministry of Higher Education of Saudi Arabia and Umm Al-Qura University for their funding support.

### REFERENCES

- Li Y, Zhou Q, Ren B, Luo J, Yuan J, Ding X *et al.*, Trends and health risks of dissolved heavy metal pollution in global river and lake water from 1970 to 2017, in *Reviews of Environmental Contamination and Toxicology*, Vol. **251**. Springer, New York, pp. 1–24 (2019).
- González-Martínez A, Simón-Martín M, López R, Táboas-Fernández R and Bernardo-Sánchez A, *Sustainability* **11**:1–27 (2019).
- Yang D, Dai C, Hu Y, Liu S, Weng L, Luo Z *et al.*, *Polymers* **9**:267 (2017).
- Ngororabanga J, Plessis JD and Mama N, *Sensors* **17**:1980 (2017).
- Grochowski C, Blicharska E, Krukow P, Jonak K, Maciejewski M, Szczepanek D *et al.*, *Front Chem* **7**:1–14 (2019).
- García M, Aguirre M and Canals A, *J Anal At Spectrom* **35**:265–272 (2020).

- 7 Eshkeiti A, Narakathu B, Reddy ASG, Moorthi A, Atashbar MZ, Rebrosov E et al., *Sens Actuators B* **171–172**:705–711 (2012).
- 8 Eddaif L, Shaban A and Telegdi J, *Int J Environ Anal Chem* **99**:824–853 (2019).
- 9 De Acha N, Elosúa C, Corres JM and Arregui FJ, *Sensors* **19**:599–632 (2019).
- 10 Johnson AD, Curtis RM and Wallace KJ, *Chemosensors* **7**:22 (2019).
- 11 Wolfbeis OS, *Chem Soc Rev* **44**:4743–4768 (2015).
- 12 Kozma E and Kele P, *Org Biomol Chem* **17**:215–233 (2019).
- 13 Wang S, Fan Y, Li D, Sun C, Lei Z, Lu L et al., *Nat Commun* **10**:1–11 (2019).
- 14 Dodani SC, He Q and Chang CJ, *J Am Chem Soc* **131**:18020–18021 (2009).
- 15 Nolan EM and Lippard SJ, *Acc Chem Res* **42**:193–203 (2009).
- 16 Divya TT, Raghav D, Rathinasamy K and Chakkumkumarath L, *New J Chem* **43**:16349–16358 (2019).
- 17 Elemans JAAW, van Hameren R, Nolte RJM and Rowan AE, *Adv Mater* **18**:1251–1266 (2006).
- 18 Wang H, Lang Y, Wang H-X, Lou J-J, Guo H-M and Li X, *Tetrahedron* **70**:1997–2002 (2014).
- 19 He X, Liu H, Li Y, Wang S, Li Y, Wang N et al., *Adv Mater* **17**:2811–2815 (2005).
- 20 Wang H, Wang D, Wang Q, Li X and Schalley CA, *Org Biomol Chem* **8**:1017–1026 (2010).
- 21 Che Y, Yang X and Zan L, *Chem Commun*:1413–1415 (2008). <http://xlink.rsc.org/?DOI=b719384j>
- 22 Çavuş S and Gürdağ G, *Ind Eng Chem Res* **48**:2652–2658 (2009).
- 23 Flaviane VP, Leandro Vinicius AG and Laurent FG, *J Hazard Mater* **176**:856–863 (2010).
- 24 Dragan ES, *Chem Eng J* **243**:572–590 (2014).
- 25 Godjevargova T, Simeonova A and Dimov A, *J Appl Polym Sci* **83**:3036–3044 (2002).
- 26 Srivastava S, *Adv Mater Lett* **4**:2–8 (2013).
- 27 Çavuş S, Yaşar G, Kaya Y, Beril Gonder Z, Gürdağ G, Vergili İ, *Process Saf Environ Pro* **103**:227–136 (2016).
- 28 Chauhan GS and Mahajan S, *J Appl Polym Sci* **86**:667–671 (2002).
- 29 Shawky HA, Ali AE-H and El Sheikh RA, *J Appl Polym Sci* **99**:2904–2912 (2006).
- 30 Zheng Y and Wang A, *J Hazard Mater* **171**:667–671 (2009).
- 31 Zheng J, Zhu L, Zhao C and Zheng J, *J Environ Anal Toxicol* **02**:1–4 (2012).
- 32 Moore JJ, Raine TP, Jenkins A, Livens FR, Law KA, Morris K et al., *React Funct Polym* **142**:7–14 (2019).
- 33 Deli D, Deli D, Law K, Liu Z, Crouch DJ, Livens FR et al., *React Funct Polym* **72**:414–419 (2012).
- 34 Xie J, Liu X and Liang J, *J Appl Polym Sci* **106**:1606–1613 (2007).
- 35 Ozay O, Ekici S, Baran Y, Kubilay S and Aktas N and Sahiner, *Desalination* **260**:57–64 (2010).
- 36 Puspitasari T, Oktaviani, Pangerteni DS, Nurfilah E and Darwis D, *Macromolecular Symposia* **353**:168–177 (2015). <https://doi.org/10.1002/masy.201550323>
- 37 Perumal S, Atchudan R, Yoon DH, Joo J and Cheong IW, *Ind Eng Chem Res* **58**:9900–9907 (2019).
- 38 Zhang M, Yin Q, Ji X, Wang F, Gao X and Zhao M, *Sci Rep* **10**:3285–3296 (2020).
- 39 Zeng Q, Qi X, Zhang M, Tong X, Jiang N, Pan W et al., *Int J Biol Macromol* **145**:1049–1058 (2020).
- 40 Morishima Y, Nomura S, Ikeda T, Seki M and Kamachi M, *Macromolecules* **28**:2874–2881 (1995).
- 41 Paek K, Chung S, Cho CH and Kim BJ, *Chem. Commun* **47**:10272–10274 (2011).
- 42 Liu Z, Liu J, Cui L, Wang R, Luo X, Barrow CJ et al., *Carbon* **51**:148–155 (2013).
- 43 Lou X, Daussin R, Cuenot S, Duwez A-S, Pagnoulle C, Detrembleur C et al., *Chem Mater* **16**:4005–4011 (2004).
- 44 Doube M, Klosowski MM, Arganda-Carreras I, Cordelières FP, Dougherty RP, Jackson JS et al., *Bone* **47**:1076–1079 (2010).
- 45 Barrett ES, Dale TJ and Rebek J, *Chem Commun*:4224–4226 (2007).
- 46 Sheng C, Wenting B, Shijian T and Yuechuan W, *J Appl Polym Sci* **125**:2867–2873 (2008).
- 47 Parviz D, Das S, Ahmed HST, Irin F, Bhattacharia S and Green MJ, *ACS Nano* **6**:8857–8867 (2012).
- 48 Kok Yetimog'lu E, Kahraman MV, Ercan O, Akdemir ZS and Apohan NK, *React Funct Polym* **67**:451–460 (2007).
- 49 Sahraei R and Ghaemy M, *Carbohydr Polym* **157**:823–833 (2017).
- 50 Chen JJ, Ahmad AL and Ooi BS, *J Environ Chem Eng* **1**:339–348 (2013).
- 51 Zhang Y, Zhang Y, Zhang Y, Wang G and He Y, *Dye Pigment* **102**:107–113 (2014).
- 52 Tolstov A, Gromadzki D, Netopilik M and Makuška R, *e-Polym* **12**:1–12 (2012).
- 53 Cui WW, Tang DY, Gong ZL and Guo YD, *J Mater Sci* **47**:6276–6285 (2012).
- 54 Calderon IAC, LKS CET, Romano E, Anore KHS, Cabatuando ACR, Ibabao MJP et al., *J Appl Polym Sci* **129**:2865–2872 (2013).
- 55 Ube T, Shin A, Aoki H and Ito S, *Langmuir* **28**:13871–13876 (2012).
- 56 Sittig M, Schmidt B, Görls H, Bocklitz T, Wächter M, Zechel S et al., *Phys Chem Phys* **22**:4072–4079 (2020).
- 57 Farhangi S, Weiss H and Duhamel J, *Macromolecules* **46**:9738–9747 (2013).
- 58 Danko M, Kasák P and Hrdlovič P, *J Photochem Photobiol A Chem* **307–308**:79–87 (2015).
- 59 Wang BC, Chang JC, Tso HC, Hsu HF and Cheng CY, *J Mol Struct (Theochem)* **629**:11–20 (2017).
- 60 Alwattar A, Haddad A, Zhou Q, Nascimento T, Greenhalgh R, Medeiros E et al., *Polym Int* **68**:360–368 (2019).
- 61 Casamayou-Boucau Y and Ryder AG, *Methods Appl Fluoresc* **5**:1–6 (2017).
- 62 Boaz H and Rollefson GK, *J Am Chem Soc* **72**:3435–3443 (1950).
- 63 De Costa MDP and Jayasing WAPA, *J Photochem Photobiol A Chem* **162**:591–598 (2004).
- 64 Chowdhury IH and Naskar MK, *Indian J Chem* **57A**:910–914 (2018).
- 65 Wang J, Mei J, Yuan W, Lu P, Qin A, Sun J et al., *J Mater Chem* **21**:4056 (2011).
- 66 Ciotta E, Proposito P, Tagliatesta P, Lorecchio C, Stella L, Kaciulis S et al., *Sensors* **18**:1496 (2018).
- 67 Yarur F, Macairan J-R and Naccache R, *Environ Sci Nano* **6**:1121–1130 (2019).
- 68 Bhuvanesh N, Suresh S, Prabhu J, Kannan K, Rajesh KV and Nandhakumar R, *Opt Mater* **82**:123–129 (2018).
- 69 Wang J, Liu F and Wei J, *Polym Bull* **67**:1709–1720 (2011).
- 70 Wang F, Zheng Y, Zhu Y and Wang A, *Water Air Soil Pollut* **227**:2–12 (2016).
- 71 Çavuş S and Yıldıran M, *Ionics* **22**:1059–1073 (2016).
- 72 Kim C and Chae JB, *J Fluoresc* **28**:1363–1370 (2018).
- 73 Sadia M, Naz R, Khan J and Khan R, *J Fluoresc* **28**:1281–1294 (2018).
- 74 De Acha N, Elosúa C and Arregui FJ, *Sensors* **20**:2–13 (2020).
- 75 Jinli Q, Takeo H and Tatsuhiro O, *Polymer* **46**:10809–10816 (2005).
- 76 Çavuş S, *J Polym Sci B Polym Phys* **48**:2497–2508 (2010).
- 77 Liao J, Liu S, Yuan Y and Zhang H, *New J Chem* **42**:5698–5708 (2018).
- 78 Illescas J, Ramírez-Fuentes YS, Zaragoza-Galán G, Porcu P, Mariani A and Rivera E, *J Polym Sci A Polym Chem* **53**:2890–2897 (2015).
- 79 Dey RE, Wimpenny I, Gough JE, Watts DC and Budd PM, *J Biomed Mater Res A* **106A**:255–264 (2018).
- 80 Kavanagh GM and Ross-Murphy SB, *Prog Polym Sci* **23**:533–562 (1998).
- 81 Li L, Yang J, Chen X and Hao X, *Synth Met* **159**:2462–2468 (2009).
- 82 Cuomo F, Cofelice M and Lopez F, *Polymers* **11**:259 (2019).
- 83 Zhang C and Eastale AJ, *J Appl Polym Sci* **94**:2083–2087 (2004).